

Quantum Attention by Overlap Interference: Predicting Sequences from Classical and Many-Body Quantum Data

Alessio Pecilli¹ and Matteo Rosati¹

¹*Dipartimento di Ingegneria Civile, Informatica e delle Tecnologie Aeronautiche,
Università degli Studi Roma Tre, Via della Vasca Navale 79, 00146 Rome, Italy*

We propose a variational quantum implementation of self-attention (QSA)—the core operation in transformers and large language models—which predicts future elements of a sequence by forming overlap-weighted combinations of past data. At variance with previous approaches, our QSA realizes the required nonlinearity through interference of state overlaps and returns a Rényi- $\frac{1}{2}$ cross-entropy loss directly as the expectation value of an observable, avoiding the need to decode amplitude-encoded predictions into classical logits. Furthermore, QSA naturally accommodates a constrained, trainable data-embedding that ties quantum state overlaps to data-level similarities. We find a gate complexity dominant scaling $O(Td^2)$ for QSA, versus $O(T^2d)$ classically, suggesting an advantage in the practical regime where the sequence length T dominates the embedding size d . In simulations, we show that our QSA-based quantum transformer learns sequence prediction on classical data and on many-body transverse-field Ising quantum trajectories—establishing trainable attention as a practical primitive for quantum dynamical modeling.

Introduction – The successful design, training and deployment of large language models, with transformer architectures as their organizing principle, is rapidly revolutionizing human activities at large [1]. The transformer is a complex neural network that takes as input sequences of data, embedded into lower-dimensional *tokens*, and outputs a prediction of the next datum in the sequence. At the heart of a transformer lies the self-attention (SA) mechanism, which compares tokens through pairwise similarities, called *attention weights*, and uses these to build collective, context-dependent predictions. At a practical level, SA is also the dominant computational bottleneck in transformers, with a characteristic quadratic dependence on sequence length [2].

These observations have motivated a rapidly growing effort to “quantize” transformer components on a quantum computer, aiming at asymptotic speedups or at quantum-enhanced expressivity [3–9]. Recent proposals span several approaches: quantization tailored to vision transformers [3]; Grover- or kernel-inspired constructions [4–6], some under structural assumptions on the attention matrix; faithful end-to-end mappings of transformer blocks onto quantum circuits [7]; approximating or replacing attention with primitives based on the quantum singular value transform (QSVT) [8, 9].

Despite this breadth of approaches, a persistent obstacle is that many quantum transformer constructions naturally store intermediate or final predictions in the amplitudes of a quantum state. While compact, this creates a practical bottleneck for training: evaluating a classical loss or decoding a next-token distribution can require additional assumptions, costly readout, or substantial classical post-processing, limiting end-to-end demonstrations. In addition, the data-to-token embedding is often left implicit, effectively assumed to be fixed in advance; however, since attention weights are built from token inner products, the embedding determines which

data-level relations are preserved and thus plays a central role in any faithful quantization of SA.

Here we introduce and study a variational quantum self-attention (QSA) mechanism that harnesses the inner-product structure of classical self-attention (CSA) and directly outputs a loss value for each data sequence, enabling efficient training. Our approach rests on three key insights: (i) the SA output is an intrinsically non-linear function of token inner products, which can be realized by a suitable non-linear encoding of tokens into quantum states; (ii) a Rényi cross-entropy loss can be estimated as the expectation of a Pauli observable via ancillary qubits, providing a hardware-friendly training signal; and (iii) a constrained yet trainable embedding links affinities between tokens to affinities between the underlying data, integrating the embedding stage into the quantization strategy. The resulting architecture, which inherits the variational structure of CSA, is naturally suited to near- and mid-term quantum hardware.

An evaluation of the gate-complexity shows that, with an amplitude-encoding of the tokens, our QSA outperforms CSA in the practically relevant regime where sequence length dominates the embedding size. Further advantages are available when the data are basis-encoded directly, bypassing explicit token embedding.

We implement our QSA and benchmark it against comparable CSA architectures in simulations of two generative modeling tasks: next-token prediction of classical sequences and prediction of quantum-state sequences generated by complex many-body Hamiltonian evolution. The latter demonstrates, for the first time to our knowledge, that attention-like mechanisms can be trained as primitives for modeling quantum dynamical sequences, providing a concrete link between quantum machine learning and Hamiltonian simulation.

Taken together, our results identify a quantum-native formulation of SA in which the essential nonlinearity

arises from interference of overlaps and the training objective is accessible as a direct measurement. This positions our QSA as a modular primitive for larger quantum machine learning pipelines [10–14]— for modeling both classical and quantum sequences, where the notion of data similarity is intrinsically an overlap of states.

Classical self-attention – In a standard language prediction task, words $\mathbf{w}_1, \dots, \mathbf{w}_{T+1}$ of a length- $(T+1)$ sequence are embedded into tokens $\mathbf{x}_i \in \mathbb{R}^d$ as follows: $\mathbf{x}_i = E\mathbf{w}_i + \mathbf{c}_i$. Here $E \in \mathbb{R}^{d \times D}$ is a rectangular matrix, representing a linear embedding layer, which maps one-hot-encoded words in the vocabulary, i.e., $\mathbf{w}_i \in \mathcal{V}$ with $\mathcal{V} := \{\mathbf{w}^{(\ell)} = (0_1, \dots, 0_{\ell-1}, 1_\ell, 0_{\ell+1}, \dots, 0_D)\}_{\ell=1}^D$, into vectors of a feature space with much smaller dimension $d \ll D$. Instead, \mathbf{c}_i are additional shifts encoding the positional information about \mathbf{w}_i in the sequence. For each training sentence, the SA layer’s output \mathbf{z}_j is given by a weighted sum of tokens up to j , with affinity weights depending on the tokens’ inner products:

$$\mathbf{z}_j = \sum_{i=1}^j \text{softmax}\left(\frac{\mathbf{q}_j \cdot \mathbf{k}_i}{\sqrt{d_K}}\right) \mathbf{v}_i, \quad (1)$$

where $\mathbf{v}_i, \mathbf{k}_i, \mathbf{q}_i$ are called value, key, and query vectors, obtained via distinct linear layers applied to \mathbf{x}_i , d_K is the key-vectors’ dimension, and the softmax operation is taken with respect to i for fixed j [2]. After the SA layer, classical transformers apply a residual connection layer, i.e., a further shift by \mathbf{x}_i , and a standard feed-forward network, with linear layers and non-linear activation function, producing a token \mathbf{z}'_i . Finally, an anti-embedding layer, comprising a linear transformation and a softmax, is applied to produce a probability vector; the latter has components $\ell = 1, \dots, D$ representing the conditional probability $p_{j+1} := P(\mathbf{w}_{j+1} = \mathbf{w}^{(\ell)} | \mathbf{w}_1, \dots, \mathbf{w}_j)$ of predicting the ℓ -th word of the vocabulary at the $(j+1)$ -th step. During training, the true next word in the sequence is known, hence the performance is evaluated via the cross-entropy loss function: $\mathcal{L}(p) := -\frac{1}{T} \sum_{j=1}^T \log(p_{j+1}/\mathcal{N}_{j+1})$, where $\mathcal{N}_{j+1} = \sum_{j=1}^T p_{j+1}$ is a normalization, and logarithms are in the natural basis.

The implementation of analogous transformations on a quantum computer, provided access to the words or tokens, faces major non-linearity issues due to two main sources: (i) non-linear combination of the tokens to calculate affinity weights in the SA layer; (ii) non-linear filtering of the tokens within or after each layer, i.e., via softmax and feed-forward networks. While source (i) is inherent to the transformer architecture, as it lies at the core of the SA mechanism, requiring a non-linearity to combine tokens based on their affinity, source (ii) is a general feature employed to increase expressivity and suitably normalize outputs in classical neural networks.

Here, we are interested in tackling the fundamental non-linearity source of SA (i), hence we will not consider source (ii), which entails removing: the softmax

non-linearity, whose use in classical networks is essential to guarantee vector normalization, a necessity automatically satisfied by the quantum computer; and the feedforward network non-linearity. If needed, both these non-linearities can be approximated via QSVT [8, 15] by operating our QSA as a subroutine.

Under these assumptions, the SA output can be redefined as

$$\tilde{\mathbf{z}}_j \propto \sum_{i=1}^j (\mathbf{q}_j \cdot \mathbf{k}_i) \mathbf{v}_i, \quad (2)$$

up to normalization. Moreover, the post-processing steps after the SA layer can be aggregated into a linear layer and a shift, mapping the SA output \mathbf{z}_j to a prediction vector $\hat{\mathbf{w}}_j \in \mathbb{R}^D$ as follows: $\hat{\mathbf{w}}_j = F(\tilde{\mathbf{z}}_j + \mathbf{x}_j)$, where $F \in \mathbb{R}^{D \times d}$ is a rectangular anti-embedding matrix. Therefore, expressing the true next word in terms of its embedded token, i.e., $\mathbf{w}_{j+1} = E^{-1}(\mathbf{x}_{j+1} - \mathbf{c}_{j+1})$, the corresponding probability can be written as an inner product: $p_{j+1} = \mathbf{w}_{j+1} \cdot \hat{\mathbf{w}}_j = (\mathbf{x}_{j+1} - \mathbf{c}_{j+1})(E^{-1})^T F(\tilde{\mathbf{z}}_j + \mathbf{x}_j)$. This expression is the sum of two terms: the $\tilde{\mathbf{z}}_j$ -dependent term can be evaluated from the SA layer’s output as an inner-product directly in feature space; instead, the \mathbf{x}_j -dependent term can be evaluated independently of $\tilde{\mathbf{z}}_j$, and it amounts to an overall shift, which can be absorbed into the positional encoding shift \mathbf{c}_j . Hence, in the absence of non-linear activations, we can also set the residual connection to zero without loss of generality, redefining the correct prediction probability as

$$p_{j+1} = \tilde{\mathbf{x}}_{j+1} G \tilde{\mathbf{z}}_j, \quad (3)$$

where we have set $\tilde{\mathbf{x}} = \mathbf{x} - \mathbf{c}$, $G = (E^{-1})^T F$.

Quantum self-attention – Our QSA is based on a key observation: the probability (3) is a fourth-degree function of the input tokens, and a quadratic function of their inner products up to variational linear transformations. Thus, leveraging an amplitude-encoding of the tokens into quantum state vectors, it is possible to construct a circuit that computes (3) efficiently, as described below.

The input to our circuit is a preparation of the state

$$|\psi\rangle = \frac{1}{\sqrt{T}} \sum_{j=1}^T |\psi_j\rangle_{AB} \otimes |j\rangle_C, \quad (4)$$

where A, B, C are the Hilbert spaces of three quantum registers with $n := \log d$ qubits each on A and B , and $t := \log(T)$ on C , while the states $\{|j\rangle\}_{j=1}^T$ form an orthonormal basis of C . Moreover, the states on AB are entangled amplitude-encodings of the input tokens:

$$|\psi_j\rangle \propto \sum_{i=1}^j |\mathbf{x}_i\rangle_A \otimes |\mathbf{x}_i\rangle_B, \quad (5)$$

with $|\mathbf{x}\rangle \propto \sum_{k=1}^d (\mathbf{x})_k |k\rangle$ a standard amplitude encoding of \mathbf{x} [16]. For simplicity, in the following derivation we omit the normalization coefficients. Note that

(5) can be constructed from $|0\rangle^{\otimes(2n+t)}$ by preparing the uniform-superposition state on C via Hadamard gates $H^{\otimes t}$ and then applying a controlled amplitude-encoding gate $\sum_j (U_{\psi_j})_{AB} \otimes |j\rangle\langle j|_C$, comprising unitaries that satisfy $|\psi_j\rangle = U_{\psi_j} |0\rangle^{\otimes 2n}$.

The circuit then applies a product of two parametric unitary layers on the data registers AB , i.e., $V_A \otimes W_B$, analogous to the linear layers that produce value, key and query vectors, and a controlled-projection onto $|\mathbf{x}_j\rangle_B$; the latter can be realized by inverting the amplitude-encoding unitary U_j , satisfying $|\mathbf{x}_j\rangle = U_j |0\rangle^{\otimes n}$, and projecting on the $|0\rangle^{\otimes n}$ state. The resulting state on AC encodes a superposition of the SA layer's outputs:

$$\langle \mathbf{x}_j |_B (V_A \otimes W_B) |\psi\rangle \propto \sum_{j=1}^T \left(\sum_{i=1}^j \langle \mathbf{x}_j | W |\mathbf{x}_i\rangle V |\mathbf{x}_i\rangle \right)_A \otimes |j\rangle_C, \quad (6)$$

where the local state on A for each j is an amplitude-encoding of $|\tilde{\mathbf{z}}_j\rangle$ from (2), having identified $V|\mathbf{x}\rangle = |\mathbf{v}\rangle$ with the amplitude-encoding of a value vector and $\langle \mathbf{x} | W |\mathbf{x}\rangle = \langle \mathbf{q} | \mathbf{k}\rangle$ with the inner product of key and query vectors. Therefore, one can obtain the inner products of the predicted tokens with the true tokens via a second controlled-projection onto $|\tilde{\mathbf{x}}_{j+1}\rangle_A = \tilde{U}_{j+1} |0\rangle^{\otimes n}$, leaving register C in the state

$$\langle (\tilde{\mathbf{x}}_{j+1})_A \otimes (\mathbf{x}_j)_B | (V_A \otimes W_B) |\psi\rangle \propto \sum_{j=1}^T \langle \tilde{\mathbf{x}}_{j+1} | \tilde{\mathbf{z}}_j \rangle |j\rangle_C. \quad (7)$$

Finally, a projection on the uniform-superposition state $(H|0\rangle)^{\otimes t}$ is realized to extract the loss function value directly. A compact circuit representation of the algorithm is shown in Fig. 1, where post-selection on the projections is rephrased as the expectation of a suitable observable on the final state $|\psi'\rangle = (\sum_{j=1}^T (\tilde{U}_{j+1}^\dagger V)_A \otimes (U_j^\dagger W)_B \otimes |j\rangle\langle j|_C) |\psi\rangle$, yielding:

$$\left\langle \left(\frac{Z + \mathbb{1}}{2} \right)^{\otimes(2n+t)} \right\rangle_{\psi'} = \left| \sum_{j=1}^T \frac{\langle \tilde{\mathbf{x}}_{j+1} | \tilde{\mathbf{z}}_j \rangle}{\sqrt{T \mathcal{N}_{j+1}}} \right|^2, \quad (8)$$

where Z is the third Pauli matrix.

Rényi- $\frac{1}{2}$ loss as an observable – We now show that the expectation (8) can be interpreted as a loss function for generative modelling. Firstly, observe that $|\langle \tilde{\mathbf{x}}_{j+1} | \tilde{\mathbf{z}}_j \rangle|^2 = p_{j+1}$ of (3), provided that G is a unitary operator that can be absorbed into the variational gate V_A ; this constrains E^{-1} and F to be isometries mapping to the same subspace of \mathbb{R}^D , i.e., $\text{ran } E^{-1} = \text{ran } F$. For example, the latter constraint is trivially satisfied if $E^{-1} \equiv F$, i.e., if the anti-embedding is precisely the inverse of the embedding; here, by constraining only the layer's range we allow for a wider variety of E, F to be optimized during training. Secondly, we can write $\langle \tilde{\mathbf{x}}_{j+1} | \tilde{\mathbf{z}}_j \rangle = \sqrt{p_{j+1}}$, provided that the overlap is real-valued; this can be guaranteed via a real-valued ansatz for the variational gates V, W , or by preceding the measurement on C with a product of variational single-qubit

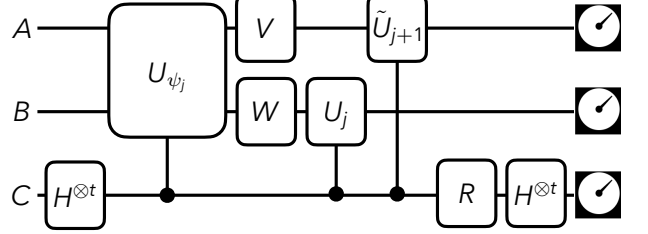


FIG. 1: Schematic depiction of our QSA circuit, as described in the text. V and W are n -qubit L -layer variational gates on each of the data registers AB , while R are products of single-qubit variational rotations, on each qubit of the ancillary register C . The controlled-gates perform amplitude-encodings of the data. The measurements estimate the expectation of $(Z + \mathbb{1})/2$ on each qubit, corresponding to the Rényi- $\frac{1}{2}$ cross-entropy loss. After training, removing the measurement of A , the last Hadamard gates, and post-selecting on the string $|j\rangle_C$, one obtains an amplitude-encoding of the predicted token $|\tilde{\mathbf{z}}_j\rangle_A$.

rotation gates R . Indeed, since $|\sum_j \sqrt{p_{j+1}} e^{i\phi_{j+1}}| \leq |\sum_j \sqrt{p_{j+1}}|$, any potential phase-set $\{\phi_{j+1}\}_j$ will be optimized to zero or to a constant. Finally, we can straightforwardly connect the right-hand side of (8) with a cross-Rényi- $\frac{1}{2}$ -entropy loss function:

$$\mathcal{L}_{\frac{1}{2}}(p) = -\log \left\langle \left(\frac{Z + \mathbb{1}}{2} \right)^{\otimes(2n+t)} \right\rangle_{\psi'} + \log T. \quad (9)$$

Here, the Rényi- α -loss is defined as $\mathcal{L}_\alpha(p) = D_\alpha(u_T||p) + H_\alpha(u_T)$, with D_α and H_α the Rényi- α divergence and entropy, and u_T the uniform distribution on T points. Note that \mathcal{L}_α equals (9) for $\alpha = \frac{1}{2}$ and the standard cross-entropy loss $\mathcal{L}(p)$ for $\alpha \rightarrow 0$. Clearly, by the non-decreasing property of the Rényi divergence with respect to α and the fact that $H_\alpha(u_T) = \log(T)$ for all α , we have that $\mathcal{L}_{\frac{1}{2}}(p) \leq \mathcal{L}(p)$, i.e., the loss function output by the QSA is a lower-bound on the standard cross-entropy.

Generative modelling of classical and quantum data sequences – We parameterize V and W with $L = 5$ layers of two-body interactions (as in [17, Fig. 2]), with gate complexity $O(Ln)$ for n qubits, and test QSA on both classical and quantum sequence-prediction tasks. We train on datasets of 300 length-5 sequences, with embedding dimension $d = 4$. As baselines, we train two CSA models with the same d and loss $\mathcal{L}_{\frac{1}{2}}$: a standard CSA (S-CSA) with unconstrained embedding and all nonlinearities, and a linear CSA (L-CSA) with the quantum-constrained embedding and no nonlinearities, computing the loss directly in token space.

For classical data, the resulting training curves are shown in Fig. 2a. Defining perplexity as $\mathcal{P} = \exp \mathcal{L}_{\frac{1}{2}}$, we

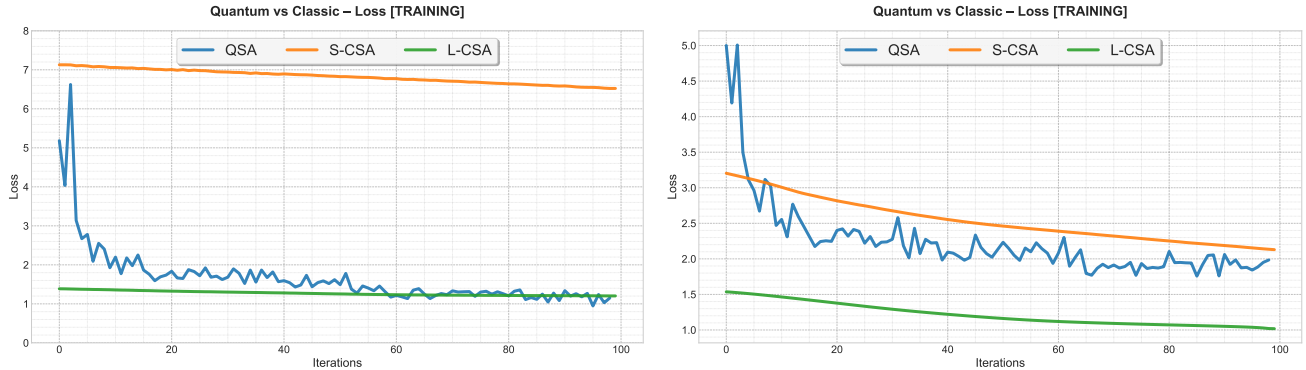


FIG. 2: Plot of the values of the loss function $\mathcal{L}_1(p)$, up to a $\log T$ constant term, vs. training epochs, for the QSA, S-CSA and L-CSA described in the text, applied to two generative modelling tasks: (a) prediction of classical data sequences; (b) prediction of quantum state evolution under transverse-field Ising Hamiltonian.

obtain $\mathcal{P}_{\text{qsa}}^{\text{train}} = 3.158$, $\mathcal{P}_{\text{s-csa}}^{\text{train}} = 680.44$, $\mathcal{P}_{\text{l-csa}}^{\text{train}} = 3.35$ on the training set, and $\mathcal{P}_{\text{qsa}}^{\text{test}} = 6.62 \pm 0.06$, $\mathcal{P}_{\text{s-csa}}^{\text{test}} = 858 \pm 1$, $\mathcal{P}_{\text{l-csa}}^{\text{test}} = 3.39 \pm 0.01$ on the test sets. We observe that QSA reaches substantially smaller loss than S-CSA; we attribute this to the constrained embedding enabling token-space loss evaluation, which is consistent with L-CSA achieving similar performance. Furthermore, the test perplexities suggest that this is not due to overfitting.

For quantum data, we sample a random $\log D$ -qubit transverse-field Ising model Hamiltonian $H = \sum_{i=1}^D X_i + \sum_{i < j} J_{ij} Z_i Z_j$ with $J_{ij} \in [0, 1]$ and $D = 10$. From random initial states $|\psi_1\rangle$ we generate sequences $|\psi_j\rangle = e^{-iH(j-1)}|\psi_1\rangle$ for $j = 2, \dots, T + 1$, identify their computational-basis amplitudes with input words \mathbf{w}_j , and feed them to QSA and the CSA baselines as above; we use an embedding layer, rather than $d = D$ equal to the Hilbert-space dimension, to retain its dimensionality-reduction features. Training curves are shown in Fig. 2b. We find $\mathcal{P}_{\text{qsa}}^{\text{train}} = 7.17$, $\mathcal{P}_{\text{s-csa}}^{\text{train}} = 6.64$, $\mathcal{P}_{\text{l-csa}}^{\text{train}} = 2.59$ on the training set, and $\mathcal{P}_{\text{qsa}}^{\text{test}} = 5.6 \pm 0.2$, $\mathcal{P}_{\text{s-csa}}^{\text{test}} = 8.4 \pm 0.6$, $\mathcal{P}_{\text{l-csa}}^{\text{test}} = 2.8 \pm 0.9$ on the test sets. Here, unlike the classical task, QSA and S-CSA are slightly outperformed by L-CSA. This behavior may depend on the Hamiltonian choice and dataset structure, highlighting a natural next step: mapping out when and how quantum self-attention is most effective for many-body dynamical prediction.

Gate complexity – Amplitude encoding an n -qubit vector costs $O(2^n)$ [16]. With $n = \log d$, the QSA cost is dominated by the controlled- U_{ψ_j} preparation, scaling as $O(Td^2)$. The L -layer variational blocks contribute $O(L \log d)$, while the classical embedding requires T matrix-vector multiplications with cost $O(TdD)$. Overall, the amplitude-encoding QSA has total complexity $O(Td(d + D) + \log d)$.

By contrast, the self-attention layer of a CSA scales as $O(Td(T + D))$ [2], with the D term accounting for the (anti)-embedding. Thus QSA is expected to be advan-

tageous when $T \gg d$, i.e., in the practically relevant regime of long sequences with fixed embedding size.

A potentially interesting variant is a basis-encoding QSA that keeps the circuit structure of Fig. 1 but operates directly on words, avoiding (anti)-embedding. Writing each $\mathbf{w}^{(\ell)} \in \mathcal{V}$ as the bit-string of its index ℓ and encoding it as $|\ell\rangle$ on $n = \log D$ qubits, a superposition of T basis states can be prepared with cost $O(Tn)$ [16], while the controlled operations scale as $O(T^2 \log D)$, still dominating. Consequently, basis-encoding QSA can outperform CSA when $d \gg \log D$, e.g., as in language-sized vocabularies, and can also outperform amplitude-encoding QSA when $d \gg T \log D$, i.e., when the sequence length is moderate relative to the embedding size.

Discussion and conclusions – We introduced a variational quantum self-attention (QSA) mechanism in which attention is implemented quantum-natively, via quantum states' inner-products, and the training objective is read out directly as an observable, bypassing the decoding bottleneck of amplitude-encoded predictions. By making embedding intrinsic to the quantization, our constrained yet trainable design ensures that token affinities track affinities in the underlying data. Our construction is readily extensible to multi-head and parallelized multilayer architectures, although developing layer-efficient implementations remains an open question. We therefore expect QSA to become an enabling primitive for quantum transformer architectures and, simultaneously, a practical tool for attention-driven modeling of many-body quantum dynamics.

Acknowledgements – M.R. acknowledges support by MUR (project FIS-2023-03472, “SuNRISE” CUP F53C24001760001).

[1] F. Calvino, J. Reijerink, and L. Samek, The effects of generative AI on productivity, innovation and entrepreneurship, *OECD Artif. Intell. Pap. OECD Artificial Intelligence Papers*, [10.1787/b21df222-en](https://doi.org/10.1787/b21df222-en) (2025).

[2] A. Vaswani, N. Shazeer, N. Parmar, J. Uszkoreit, L. Jones, A. N. Gomez, L. Kaiser, and I. Polosukhin, Attention Is All You Need, [arXiv preprint arXiv:1706.03762](https://arxiv.org/abs/1706.03762) (2017).

[3] E. A. Cherrat, I. Kerenidis, N. Mathur, J. Landman, M. Strahm, and Y. Y. Li, Quantum Vision Transformers, *Quantum* **8**, 1265 (2022), [arXiv:2209.08167](https://arxiv.org/abs/2209.08167).

[4] Y. Gao, Z. Song, X. Yang, and R. Zhang, Fast Quantum Algorithm for Attention Computation, [arXiv preprint arXiv:2307.08045](https://arxiv.org/abs/2307.08045) (2023).

[5] R.-X. Zhao, J. Shi, and X. Li, GQHAN: A Grover-inspired Quantum Hard Attention Network, [arXiv preprint arXiv:2401.14089](https://arxiv.org/abs/2401.14089) (2024).

[6] R.-X. Zhao, J. Shi, and X. Li, QKSAN: A Quantum Kernel Self-Attention Network, *IEEE Trans. Pattern Anal. Mach. Intell.* **46**, 10184 (2024).

[7] Y. Liao and C. Ferrie, GPT on a Quantum Computer, [arXiv preprint arXiv:2403.09418](https://arxiv.org/abs/2403.09418) (2024).

[8] N. Guo, Z. Yu, M. Choi, A. Agrawal, K. Nakaji, A. Aspuru-Guzik, and P. Rebentrost, Quantum linear algebra is all you need for Transformer architectures, [arXiv preprint arXiv:2402.16714](https://arxiv.org/abs/2402.16714) (2024).

[9] N. Khatri, G. Matos, L. Coopmans, and S. Clark, Quixer: A Quantum Transformer Model, [arXiv preprint arXiv:2406.04305](https://arxiv.org/abs/2406.04305) (2024).

[10] R. Puig, M. Drudis, S. Thanasilp, and Z. Holmes, Variational Quantum Simulation: A Case Study for Understanding Warm Starts, *PRX Quantum* **6**, 010317 (2025).

[11] M. Cerezo, G. Verdon, H.-Y. Huang, L. Cincio, and P. J. Coles, Challenges and opportunities in quantum machine learning, *Nat. Comput. Sci.* **2**, 567 (2022).

[12] M. Rosati and A. Solana, Joint-detection learning for optical communication at the quantum limit, *Opt. Quantum* **2**, 390 (2024), [arXiv:2312.13693](https://arxiv.org/abs/2312.13693).

[13] M. Bilkis, M. Rosati, and J. Calsamiglia, Reinforcement-learning calibration of coherent-state receivers on variable-loss optical channels, in *2021 IEEE Inf. Theory Work.* (IEEE, 2021) pp. 1–6.

[14] M. Rosati, A learning theory for quantum photonic processors and beyond, *Quantum* **8**, 1433 (2024), [arXiv:2209.03075](https://arxiv.org/abs/2209.03075).

[15] A. G. Rattew and P. Rebentrost, Non-Linear Transformations of Quantum Amplitudes: Exponential Improvement, Generalization, and Applications, [arXiv preprint arXiv:2309.09839](https://arxiv.org/abs/2309.09839) (2023).

[16] M. Schuld and F. Petruccione, *Supervised Learning with Quantum Computers*, Quantum Science and Technology (Springer International Publishing, Cham, 2018).

[17] R. LaRose, A. Tikkoo, É. O’Neil-Judy, L. Cincio, and P. J. Coles, Variational quantum state diagonalization, *npj Quantum Inf.* **5**, 57 (2019).